AD-A119 786 AEROSPACE CORP EL SEGUNDO CA SPACE SCIENCES LAB F/G 20/5
PULSED DF CHAIN-LASER BREAKDOWN INDUCED BY MARITIME AEROSOLS.(U)
AUG 82 S T AMIMOTO, J S WHITTIER F04701-81-C-0082
UNCLASSIFIED TR-0082(2720)-1 SD-TR-82-61 NL

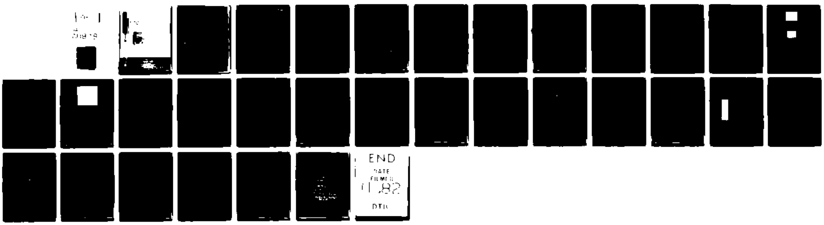

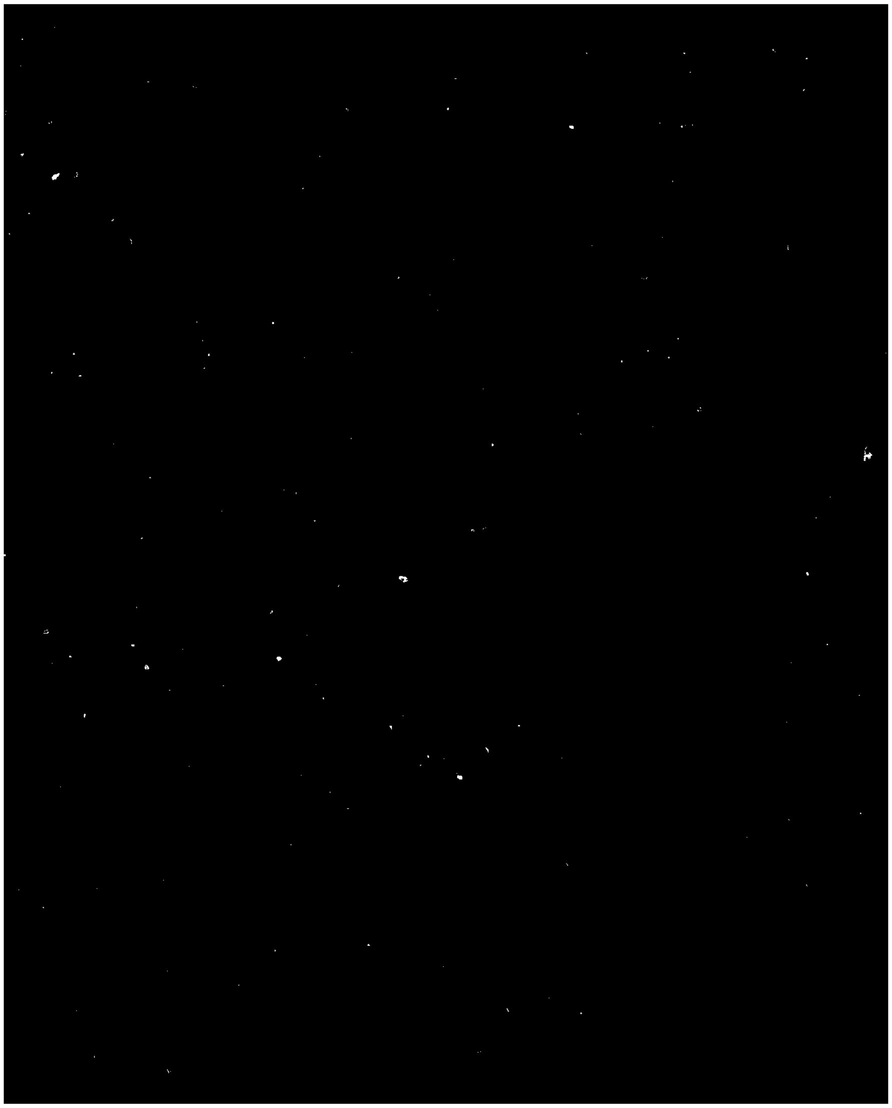

This report was submitted by The Aerospace Corporation, El Segundo, CA 90245, under Contract No. F04701-81-C-0082 with the Space Division, Deputy for Technology, P.O. Box 92960, Worldway Postal Center, Los Angeles, CA 90009. It was reviewed and approved for The Aerospace Corporation by W. P. Thompson, Director, Aerophysics Laboratory. Lt Efren V. Fornoles, SD/YLXT, was the project officer for Technology.

This report has been reviewed by the Public Affairs Office (PAS) and is releasable to the National Technical Information Service (NTIS). At NTIS, it will be available to the general public, including foreign nations.

This technical report has been reviewed and is approved for publication. Publication of this report does not constitute Air Force approval of the report's findings or conclusions. It is published only for the exchange and stimulation of ideas.

Efren V. Fornoles

Efren V. Fornoles, 2nd Lt, USAF
Project Officer

Jimmie H. Butler

Jimmie H. Butler, Colonel, USAF
Director of Space Systems Technology

FOR THE COMMANDER

Norman W. Lee, Jr.

Norman W. Lee, Jr., Colonel, USAF
Deputy for Technology

UNCLASSIFIED

SECURITY CLASSIFICATION OF THIS PAGE (When Data Entered)

REPORT DOCUMENTATION PAGE

READ INSTRUCTIONS BEFORE COMPLETING FORM

1. REPORT NUMBER SD-TR-82-61	2. GOVT ACCESSION NO. AD-A229786	3. RECIPIENT'S CATALOG NUMBER
4. TITLE (and Subtitle) PULSED DF CHAIN-LASER BREAKDOWN INDUCED BY MARITIME AEROSOLS		5. TYPE OF REPORT & PERIOD COVERED
		6. PERFORMING ORG. REPORT NUMBER TR-0082(2720)-1
7. AUTHOR(s) S. T. Amimoto, J. S. Whittier, F. G. Ronkowski, P. R. Valenzuela, G. N. Harper, R. Hofland, Jr., G. L. Trusty, T. H. Cosden, and D. H. Leslie		8. CONTRACT OR GRANT NUMBER(s) F04701-81-C-0082
9. PERFORMING ORGANIZATION NAME AND ADDRESS The Aerospace Corporation El Segundo, Calif. 90245		10. PROGRAM ELEMENT, PROJECT, TASK AREA & WORK UNIT NUMBERS
11. CONTROLLING OFFICE NAME AND ADDRESS Naval Research Laboratory Washington, D.C. 20375		12. REPORT DATE 30 August 1982
		13. NUMBER OF PAGES 27
14. MONITORING AGENCY NAME & ADDRESS (if different from Controlling Office) Space Division Air Force Systems Command Los Angeles, Calif. 90009		15. SECURITY CLASS. (of this report) Unclassified
		15a. DECLASSIFICATION/DOWNGRADING SCHEDULE

16. DISTRIBUTION STATEMENT (of this Report)

Approved for public release; distribution unlimited

17. DISTRIBUTION STATEMENT (of the abstract entered in Block 20, if different from Report)

18. SUPPLEMENTARY NOTES

micron

19. KEY WORDS (Continue on reverse side if necessary and identify by block number)

Propagation
Pulsed DF chain laser
Aerosol breakdown
Water aerosols
Alumina aerosols

micron

micron

20. ABSTRACT (Continue on reverse side if necessary and identify by block number)

Thresholds for breakdown induced by liquid and solid aerosols in room air have been measured for a 1 μsec-duration pulsed D_2-F_2 laser of 3.58 -4.78 μm bandwidth. The DF laser beam was directed into an aerosol chamber that simulated maritime atmospheres on the open sea. Both focused and collimated beams were studied. For a focused beam in which the largest encountered aerosol particles were of 1 to 4 μm diameter, pulsed DF breakdown thresholds were measured to lie in the range 0.6 to 1.8 GW/cm^2. Salt-water aerosol breakdown thres-

DD FORM 1473 (FACSIMILE)

UNCLASSIFIED

SECURITY CLASSIFICATION OF THIS PAGE (When Data Entered)

AEROSPACE FORM 4341-1 REV 5-74

19. KEY WORDS (Continued)

Plasma growth rate
Breakdown threshold theory
Maritime aerosol distributions
Long-path pulsed-laser transmission

micro

sq cm

sq cm

20. ABSTRACT (Continued)

holds for micron-size particles were found to be 15 to 30% higher than the corresponding thresholds for fresh-water particles. For a collimated beam that encountered particle diameters as large as 100 μm, breakdown could not be induced using 0.5-μsec (FWHM) pulses at peak intensities of 59 MW/cm^2. Image converter camera measurements of the radial plasma growth rate of 1.3 cm/μsec (at 1.4 GW/cm^2) were consistent with measurements of the cutoff rate of the transmitted laser beam. Pulsed DF breakdown thresholds of 32 MW/cm^2 for 30-μm diameter Al_2O_3 particles were also measured to permit comparison with the earlier pulsed-HF breakdown results of Lencioni, et al.; the solid-particle threshold measurements agree with the Lencioni data if one assumes that the thresholds for microsecond-duration pulses scales is λ^{-1}. An approximate theoretical model of the water particle breakdown process is presented that permits the scaling of the present results to other laser pulse durations, aerosol distributions, and transmission path lengths. The model is shown to be in satisfactory agreement with the experimental data.

sq cm

micro

1/lambda

AEROSPACE FORM 4341-2 REV 5-74

PREFACE

The authors gratefully acknowledge the contributions of Prof. M. Bass of USC for his experimental assistance and encouragement during the course of the research reported herein. Dr. S. K. Searles of the Naval Research Laboratory was the technical monitor, and Dr. R. Hofland of The Aerospace Corporation was the principal investigator.

CONTENTS

FIGURES

TABLE

I. INTRODUCTION

Laser plasma ignition by aerosol particles limits the optical intensities that can be propagated through the atmosphere. Above the breakdown threshold, aerosol particles ignite intense plasmas that are opaque to visible and infrared irradiation. These plasmas grow rapidly and may fully block the laser beam, depending upon the number density of breakdowns, the plasma radial growth rate, and the laser pulse duration. Previous experimental and theoretical work on the aerosol-induced breakdown problem has been carried out primarily at CO_2 laser wavelengths (10.6 μm).[1-6] Here it has been shown that (1) aerosol particles lower the breakdown threshold below the clean air value, (2) threshold reduction is relatively insensitive to aerosol particle material, except for the case of water aerosols that cause a significantly smaller reduction in threshold than do solid-particle aerosols, and (3) for large-diameter particles breakdown threshold decreases with both increasing particle size and increasing laser pulse duration. At pulsed-HF chain-laser wavelengths, thresholds for air breakdown initiated by various solid aerosols have been measured using a long-pulse-duration (3.5 μsec) laser beam.[7] Measured thresholds were found to be higher by factors of 3 to 5 than the corresponding 10.6-μm data, suggesting a breakdown threshold dependence on wavelength of $I_B \sim \lambda^{-1}$. This result contrasts sharply with short pulse data,[5,8] where the threshold for large particles has been found to scale as λ^{-2}. Recently, a pulsed DF-laser threshold measurement was reported for clean helium;[9] earlier, short-pulse HF and DF laser breakdown of air was studied by two groups.[10a,10b] Aside from that work, we are aware of no breakdown data that have been published at the laser wavelengths employed in the present study.

The results of a brief (three-week) experimental study of long-pulse breakdown induced by maritime and solid-particle aerosols at pulsed-DF chain-laser wavelengths (3.58 to 4.78 μm) are reported here. Threshold measurements in maritime aerosols have been performed using both collimated and focused beams, bracketing the intensity range of breakdown-free propagation over long transmission paths. Radial and axial growth rates of the aerosol initiated plasmas have also been measured. An approximate theoretical model of the aerosol breakdown process that considers aerosol vaporization and subsequent cascade ionization by the laser beam is shown to be in reasonable agreement with the experimental data and, in principle, permits scaling of the laboratory breakdown data tc long propagation paths.

II. EXPERIMENTAL TECHNIQUE

A magnetically confined electron beam was used to initiate the pulsed chain-reaction DF laser.[11] Mixtures containing $20\%F_2$-$8\%D_2$ by volume were irradiated for periods of approximately 0.5 μsec at current densities of 20 A/cm^2 to accomplish laser initiation. Nominal laser energies of 30 J in 0.8-μsec (FWHM) pulses were delivered at cavity pressures of 800 Torr. Laser energy and pulse duration variations were accomplished through adjustment of the laser cavity pressure. Energy was extracted from the gain medium by means of a transmission-coupled half-symmetric unstable resonator and then collimated using a CaF_2 lens of 8-m focal length. Burn patterns on calibrated witness film indicated a highly uniform intensity profile in the near-field output beam. The beam was propagated a distance of about 100 meters through an insulated duct to the vicinity of the aerosol generator.

The experimental configuration in the area of the aerosol chamber is shown in Fig. 1. Two CaF_2 wedges were used to sample the incident and transmitted laser energy and irradiance time history on each breakdown experiment. Laser pulse energies were measured using ballistic thermopiles, and emission time profiles of the laser pulse were monitored with Au:Ge detectors. Both collimated and focused beams were directed into the aerosol chamber. A 3:1 reducing telescope consisting of a 3-m-radius concave mirror and a 1-m-radius convex mirror was used to generate a collimated beam. Substitution of a flat mirror for the convex-mirror element in the telescope permitted the laser beam to be brought to a focus within the aerosol generator.

Three techniques were employed in the observation of aerosol breakdowns. An open-shutter camera was used to provide unequivocal photographic evidence of breakdown in the aerosol chamber. The onset of ultraviolet emission from breakdown plasmas was monitored using a 1P28 photomultiplier tube. Rapid cutoff of the transmitted DF beam was observed to follow closely the onset of ultraviolet plasma emission. This sequence of events is illustrated in the oscillograms of Fig. 2. For the case shown, full beam blockage is observed to occur in the transmitted irradiance record approximately 100 nsec after the ultraviolet emission record shows the first evidence of plasma formation.

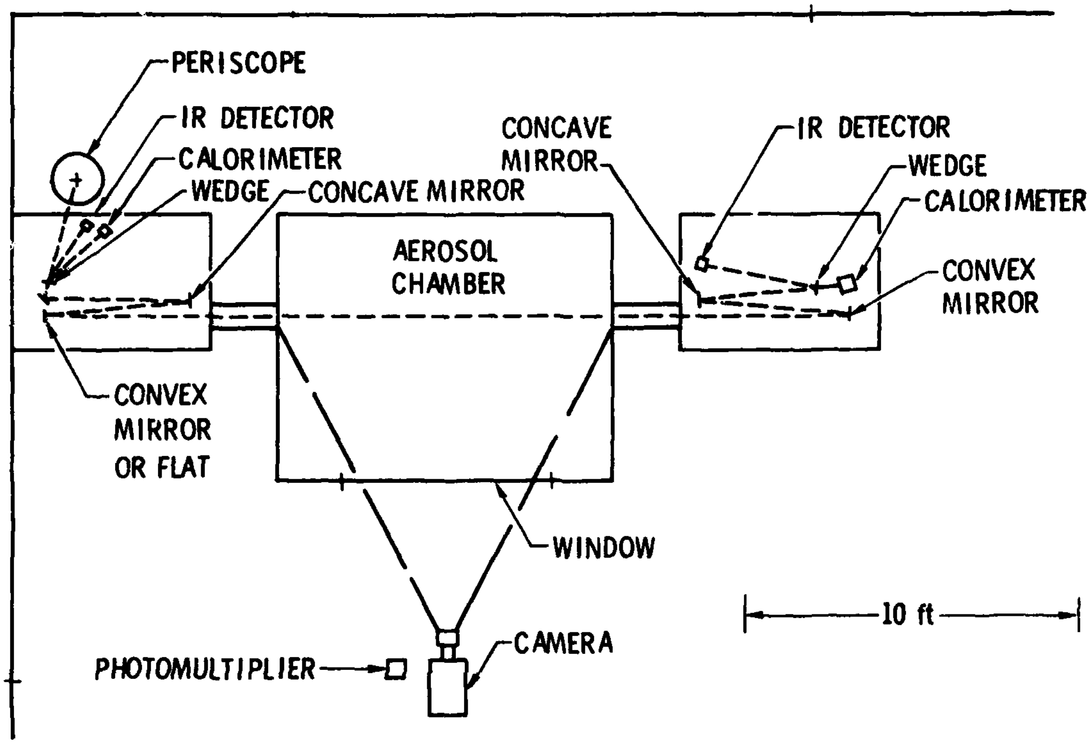

Fig. 1. Experimental Arrangement in Aerosol Chamber Laboratory

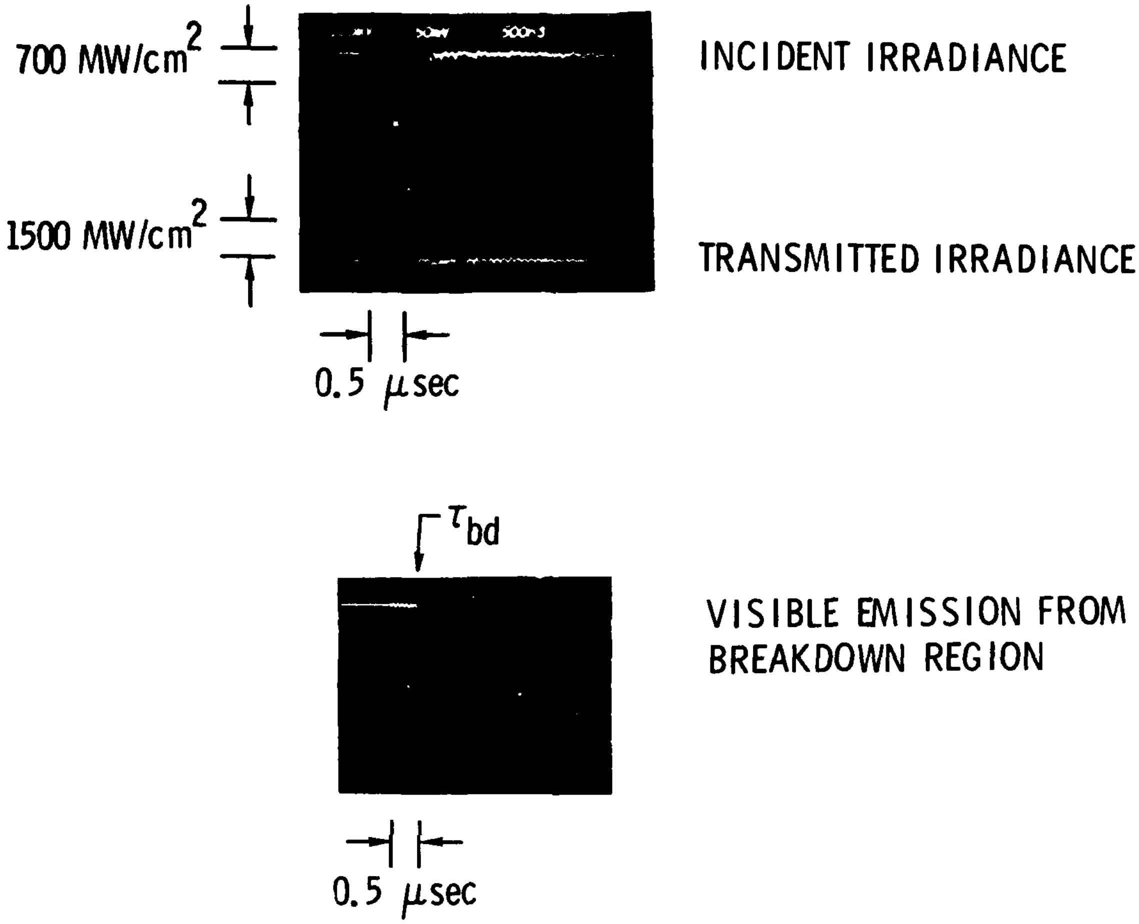

Fig. 2. Oscillograms of Incident Irradiance, Transmitted Irradiance, and Plasma Ignition Onset

Aerosol plasma growth rates were obtained using image converter camera data. Framing rates of 10^6 or 2×10^7 sec^{-1} were employed; the exposure time at a 20-MHz framing speed is 10^{-8} sec. A discussion of the data obtained with the image converter camera is presented later.

The spatial distribution of radiation in the breakdown region was determined using burns on exposed, developed photographic film. For the focused beam case, a Gaussian irradiance distribution, $I(r,z,t) = I_0(t) \exp[(r/w)^2]$ was assumed, and from the burns we determined w. The centerline fluence ε_c was calculated from the measured pulse energy E_p and w according to the relationship

$$\varepsilon_c = \varepsilon(r = 0, z) = \lim_{r \to 0} \int_0^\infty I(r,z,t)dt = \frac{E_p}{\pi w^2(z)} \tag{1}$$

The centerline irradiance at breakdown was determined from the expressions

$$I_B = I(r = 0, z, t_B) = kv(t_B) \tag{2}$$

$$k = \frac{\varepsilon_c}{\int_0^\infty v(t)dt} \tag{3}$$

where k (W/cm^2-V) is the proportionality factor relating the incident irradiance and the detector output voltage, and t_B is the time to breakdown as determined from the photomultiplier measurement of plasma emission onset. The accumulated centerline fluence at breakdown was obtained from the equation

$$\varepsilon_B = \varepsilon(r = 0, z, t_B) = \int_0^{t_B} I_0(t)dt \tag{4}$$

The irradiance waveforms were digitized to perform numerical evaluation of the integrals in Eqs. (3) and (4). For the collimated-beam (near-field) case, the transmission-coupled unstable resonator produced a nearly uniform spatial fluence and irradiance distribution such that $\varepsilon_c \cong \bar{\varepsilon} = E_p/A_{burn}$ and $I_0 \cong \bar{I} = kv(t)$. A film burn that illustrates the uniformity of the resonator near-field fluence distribution is shown in Fig. 3.

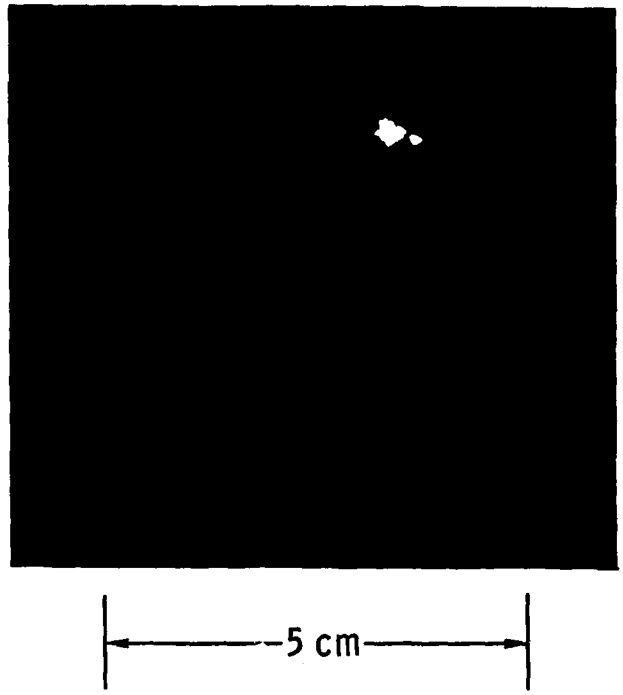

Fig. 3. Near-Field Burn of Pulsed DF Laser Output

An aerosol generator was used to simulate representative maritime and fog-bank conditions on the open ocean.[12] A 3.6 by 2.3 by 2.1 m metal enclosure was internally fitted with four nozzle heads and three spinning disk humidifiers for dispensing salt- or fresh-water aerosols. After a transient period of about 30 min, it was found that a temporally stable distribution could be achieved. Relatively uniform spatial aerosol distributions within the enclosure were obtained by use of a circulation fan. The enclosure was fitted with ports on three of its sides that were opened several seconds before an experiment to permit laser-beam and camera access to the particle-laden air. Three particle spectrometers were installed within the chamber to sample aerosol size distributions between 0.1 and 200 μm. Data from the sensors were recorded on magnetic tape at 1-sec intervals and fed to a PDP-11/34 data acquisition system for real-time processing. Output from the computer included aerosol size distributions, from the probe data, and the calculation of particle number density. An actual probe measurement and calculation using the above system is illustrated in Fig. 4a for the case of a fog-bank simulation by the aerosol generator. The plot presents $dN/dR(cm^{-3}\ \mu m^{-1})$, where N is particle concentration and R is particle radius, versus R using logarithmic coordinates. The "squares" in Fig. 4a indicate the range of the active scattering probe, and the "triangles" and "crosses" indicate the ranges of the two high-volume scattering probes. Also included in Fig. 4a is a calculation of $N(>R_o) = \int_{R_o}^{\infty} dR \times dN/dR$, the number density of particles with radii that exceed R_o. Figure 4b illustrates the results of probe measurements of an aerosol distribution that closely simulates a maritime condition of the type reported in Ref. 12. In general, breakdown measurements were carried out in the fog bank aerosol distributions illustrated in Fig. 4a.

For solid-particle aerosol breakdown experiments, a nitrogen gas-driven fluidized-bed injector was constructed to produce a uniform Al_2O_3 aerosol suspension. Alumina particles of 20 μm diameter were selected for use with the nitrogen-driven aerosol generator. Aerosol density in the breakdown region was sufficiently large to provide numerous Al_2O_3 particles in the focal volume, but small enough that diffractive fill-in was insured.

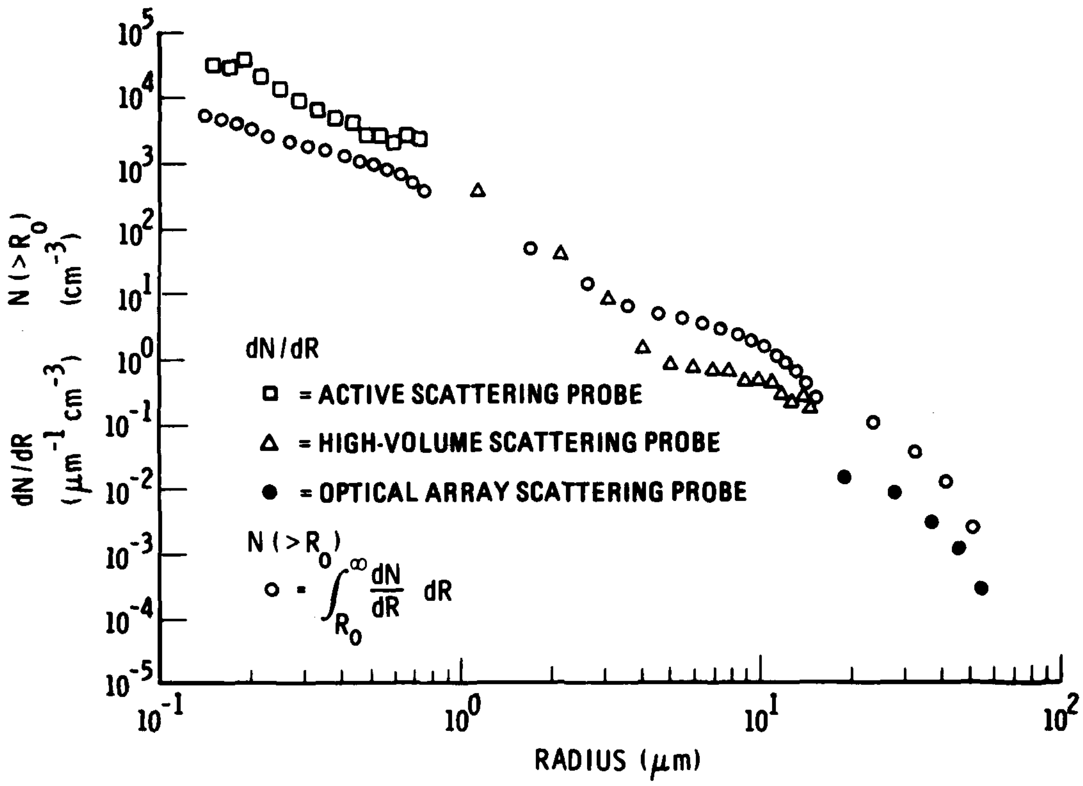

Fig. 4a. Aerosol Size Distribution Measurement for Fog-Like Maritime Environment

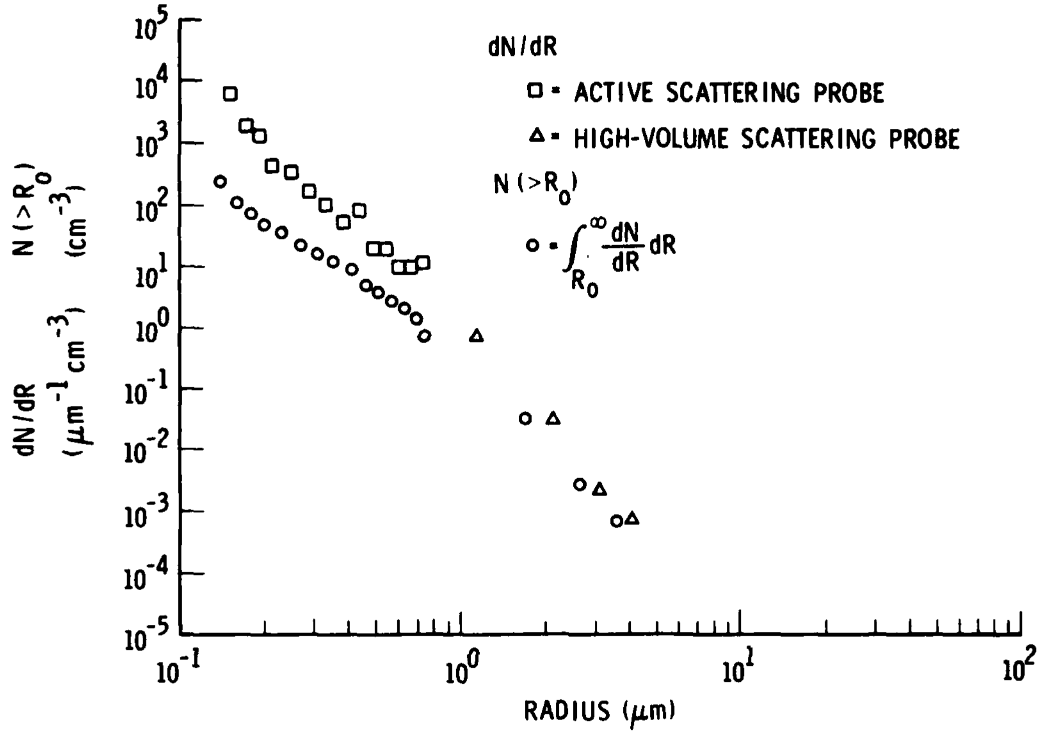

Fig. 4b. Aerosol Size Distribution Measurement for Typical Maritime Environment

III. RESULTS AND DISCUSSION

The breakdown measurements carried out during the present study are summarized in Table 1. The values of breakdown threshold I_B correspond to those values of centerline irradiance at the focal plane, which produce a high (~90%) probability of breakdown. The accumulated fluence at the time of breakdown is also shown for cases where an unequivocal determination of breakdown time could be made. The estimated uncertainty in the reported thresholds is ±30%. The error is dominated by the uncertainty in the spatial beam profile at the breakdown location.

For the collimated beam case shown in Table 1, we were unable to achieve breakdown at peak centerline irradiances of 59 MW/cm^2 in a fog-like aerosol distribution. From the measured aerosol distribution function, the largest particle diameter in the irradiated volume was calculated to be 100 μm. During this experiment, the laser irradiance exceeded 50 MW/cm^2 for a 500-nsec portion of the pulse. Assuming the threshold scales as $\tau_{\nu}^{-0.5}$, we infer a safe irradiance for a t-(μsec) duration pulse propagating through aerosols of 100 μm diameter or smaller to be $35[t(\mu sec)]^{-0.5}$ MW/cm^2.

Breakdown experiments were performed using 20-μm-diameter Al_2O_3 particles suspended in the focal region of the DF beam in order to gain confidence in the present experimental technique. A 4.5-μsec (FWHM) laser pulse was employed for these breakdown tests. The measured threshold of 32 MW/cm^2 shown in Table 1 is plotted in Fig. 5 along with the recent long-pulse (3.5 μsec) data of Lencioni et al. at HF and CO_2 wavelengths.[4,7] Assuming that λ^{-1} scaling is valid in the present regime, the present threshold measurement is in excellent agreement with the experimental results of Lencioni et al.

Two kinds of breakdown experiments are summarized in Table 1 for fog-like distributions and focused beams. In the first class of experiments (Runs 727 and 742), the laser cavity pressure and, consequently, the pulse energy were reduced in small increments, using temporally flat-topped laser irradiance profiles, until breakdown was observed to cease. This approach yielded the smallest measured values of breakdown threshold. Note that in Table 1 the

Table 1. Aerosol Breakdown Summary

Run	Aerosol	Beam	Volume (cm^3)	Largest Part Diameter	t_B (μsec)	I_b (MW/cm^2)	ε_B (J/cm^2)
712	Fog (Fresh)	Collimated	110	102	>1/2	>59	>39
727	Fog (Fresh)	Focused	8×10^{-3}	1.5	-	620	-
742	Fog (Salt)	Focused	8×10^{-3}	2.6-4	0.41-1	710-855	-
758	Al_2O_3	Focused	8×10^{-3}	20	-	32	-
778	Fog (Fresh)	Focused	8×10^{-3}	1.5	0.4	1605	320
779	Fog (Fresh)	Focused	8×10^{-3}	1.5	0.39	1850	795
780	Fog (Fresh)	Focused	8×10^{-3}	1.5	0.41	1640	475

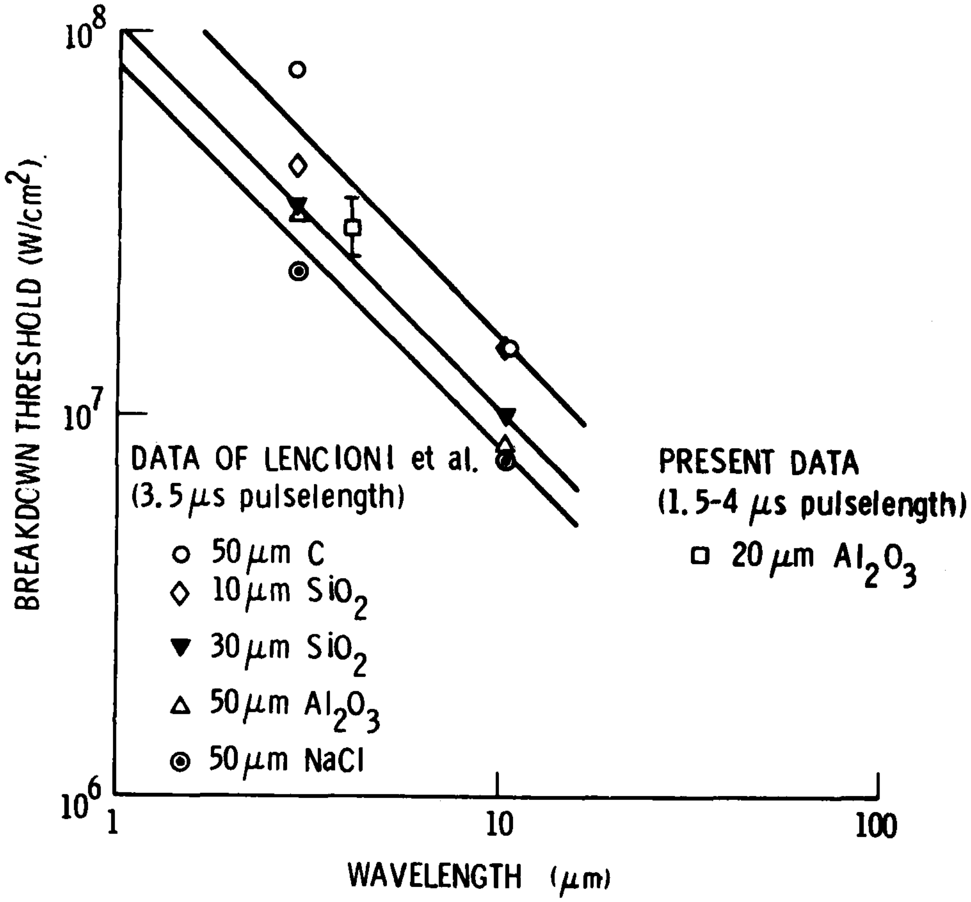

Fig. 5. Present Measurement of Alumina Breakdown Threshold Compared with Data of Lencioni et al.

threshold for salt-water aerosols is somewhat higher than that for fresh-water aerosols, even though larger particle sizes were sampled in the salt-water aerosol case. In the second class of experiments (Runs 778 through 780), the laser was operated at 800-Torr cavity pressure, yielding peak irradiances that were at least five times higher than the previously measured breakdown thresholds. In this class of experiments, breakdowns were observed at times for which the incident irradiance was still increasing rapidly with time. The irradiances at which breakdowns were observed in these experiments were approximately two and one-half to three times greater than the values measured by the prior method. That significant differences were observed in measured breakdown thresholds for the two classes of pulses was not unexpected. If the time to attain breakdown for the fast-rising pulse is τ_B' and if τ_B is the time at which the fast-rising pulse crosses the flat-topped threshold irradiance, then the threshold I_B' for the fast-rising pulse can be related to the flat-topped threshold I_B by the expression

$$I_B' = I_B + \frac{dI}{dt}(\tau_B' - \tau_B)$$

Inserting typical values for dI/dt (5 MW/cm^2-nsec), I_B' (1.6 GW/cm^2) and I_B (0.6 GW/cm^2), one finds that $\tau_B' - \tau_B = 200$ nsec. The latter time is the effective aerosol breakdown time for the fast-rising pulse. It is far shorter than the breakdown time for the flat-topped pulse because of the higher effective irradiance acting during the vaporization and avalanche phases of the fast-rising pulse. These data highlight the important role that the laser pulse shape plays in the determination of a threshold value of the breakdown irradiance.

The breakdown irradiance data of Table 1 are plotted in Fig. 6 as a function of aerosol particle diameter. Included in Fig. 6 are the recent long-pulse HF data of Lencioni et al.[7] and an unpublished theoretical breakdown calculation[13] that extends the treatment of Smith[14] to include electron attachment to water vapor and molecular oxygen. Briefly, the vapor density leaving the aerosol surface as a result of laser irradiation of the particle is determined in the model, and the irradiance required to cascade ionize the

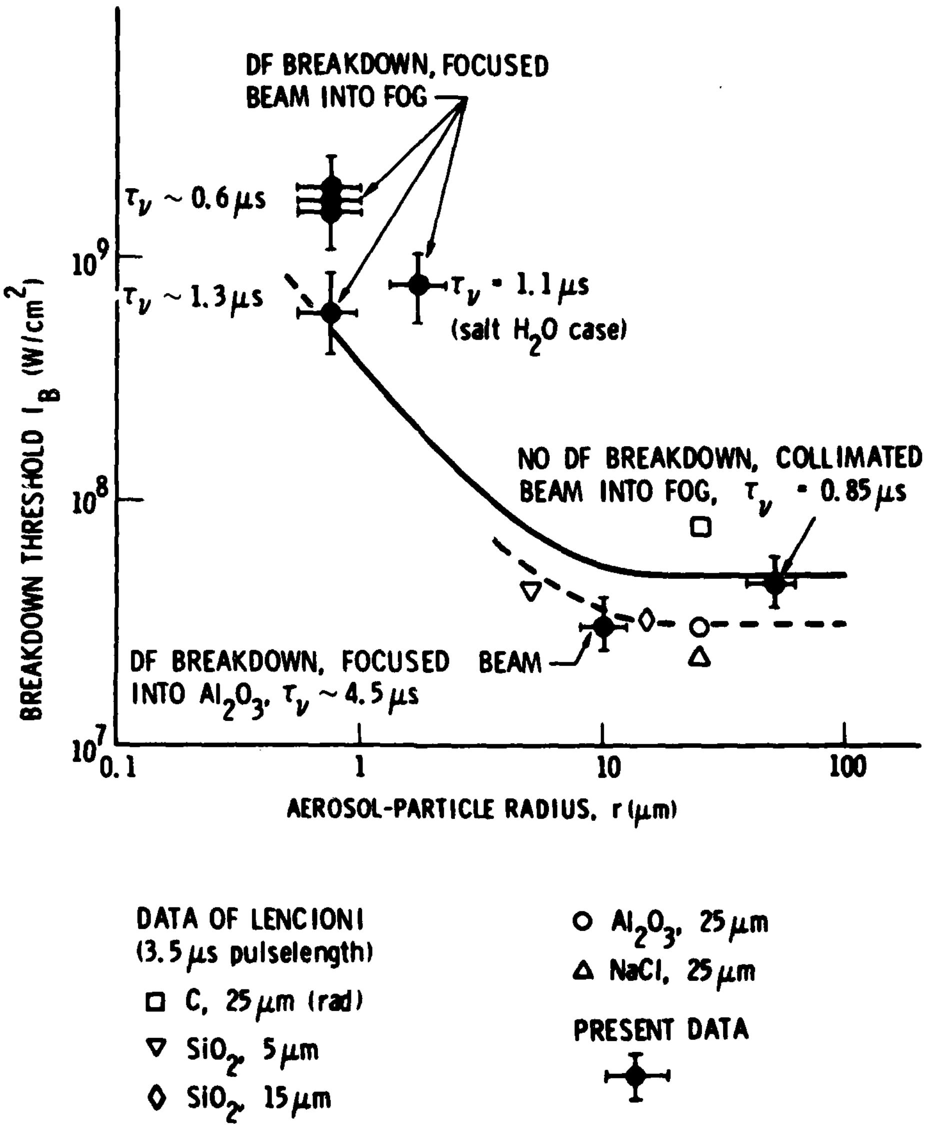

Fig. 6. Pulsed Chemical Laser Breakdown Threshold Versus Aerosol Size: Theory and Experiment

vapor to complete ionization is calculated. Qualitatively speaking, smaller particles are more difficult to ionize because of their low absorption efficiency and high rate of electron loss by free and ambipolar diffusion. For aerosol particles larger than 7 μm, elastic heating and attachment losses dominate over diffusion losses under present conditions. The predicted DF threshold for nominal 1-μsec-duration pulses is plotted in Fig. 6 as the solid curve, while the dotted curve is the predicted HF threshold for nominal 4-μsec-long pulses. The agreement between theory and experiment is considered satisfactory considering the simplified nature of the model and the experimental error in the determination of particle size and breakdown threshold.

The data presented Fig. 6 have been used to construct the crude map shown in Fig. 7 of the DF breakdown threshold as a function of particle size and time to breakdown. Implicit in the construction of Fig. 7 is the assumption that the DF thresholds are relatively insensitive to particle material as has been found to be the case at HF and CO_2 wavelengths. Included in the figure are the DF clean-air breakdown data of Deka et al.[10a] and the results of our wavelength scaling of the data of Lencioni et al.[5,7] Considerable liberty has been taken in estimating the position of the curves according to particle size. It should be emphasized that much additional data must be generated before the empirical correlation of Fig. 7 has a firm experimental basis for DF wavelengths.

A typical series of image converter frames that depict the breakdown spatial growth rate at irradiances above the breakdown threshold is shown in Fig. 8. The dashed lines in the frames mark the e^{-1} diameter of the laser beam, which we estimate to be 1.6 mm. The laser pulse is incident from the bottom of Fig. 8. Two breakdowns can be observed in the first two frames. The lower breakdown starts near the center of the beam and grows radially to completely fill the beam after about three frames. The inferred radial expansion velocity is consistent with the observed delay time between cutoff of the transmitted laser pulse and the initial observation of plasma ignition. As time progresses, the upper breakdown plasma is shielded by the lower breakdown; it is completely extinguished by the third frame. The lower breakdown plasma is observed to form an inverted-pyramid shape as it selectively absorbs

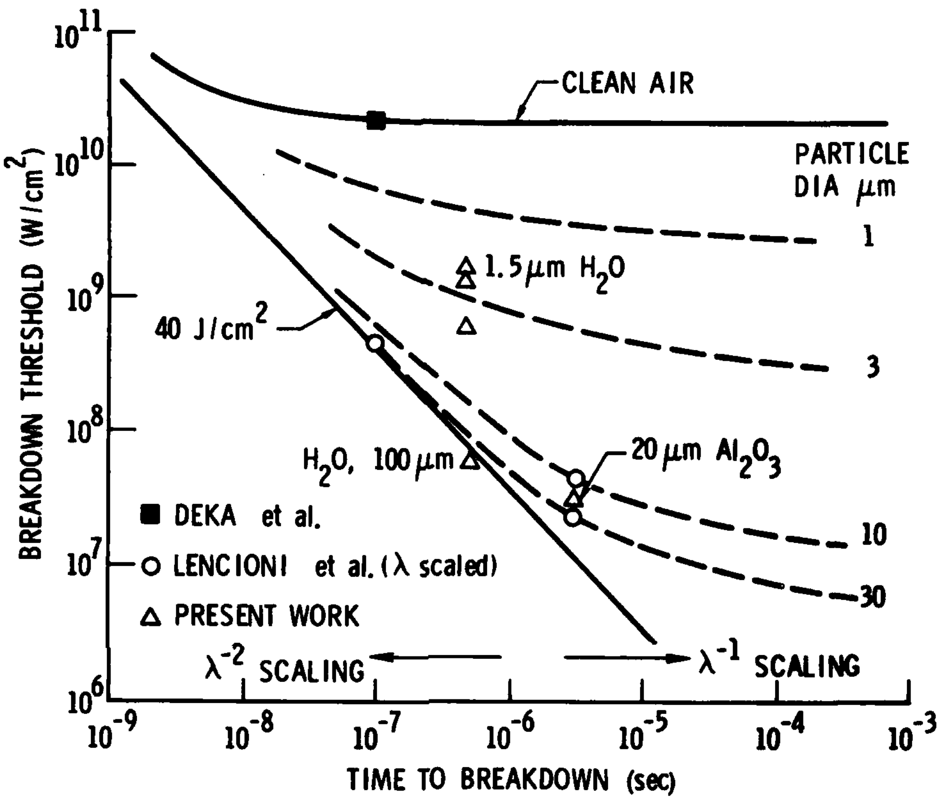

Fig. 7. Estimated Air Breakdown Thresholds for DF Laser Pulses

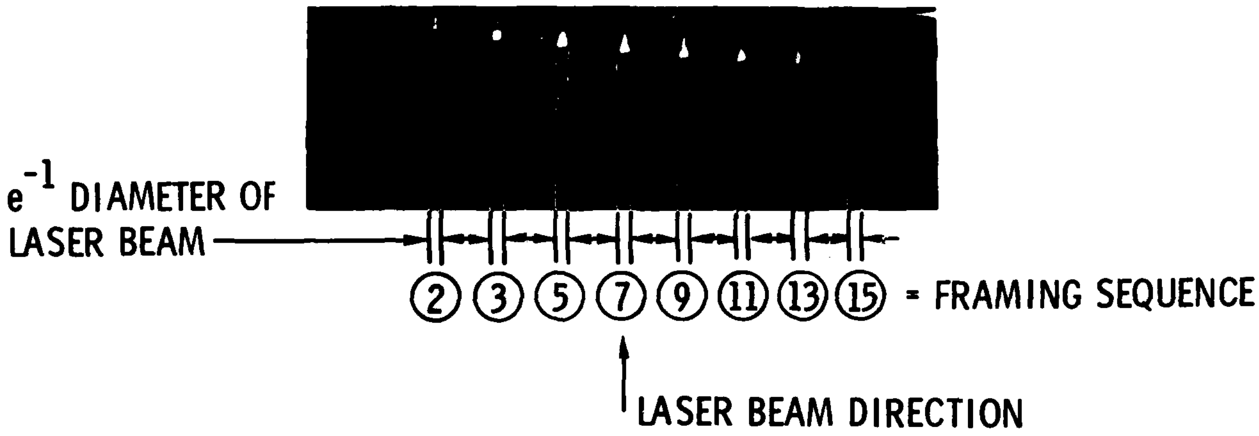

FRAMING RATE = 5×10^7 sec^{-1}

Fig. 8. Framing Photographs of Breakdown Growth

radiation at its front surface and propagates back toward the laser source. This behavior is characteristic of a laser-supported detonation (LSD) wave.[15]

Radial and axial velocities of the expanding breakdown plasmas have been calculated from the experimental data of Fig. 8. These results are presented in Fig. 9 along with data obtained at CO_2 wavelengths.[16] Included in Fig. 9 are the theoretical predictions of Raizer for the radial and axial plasma growth rates. Although the data lie somewhat above the predicted velocities, agreement between theory and experiment is considered reasonable. At 1 GW/cm^2 irradiance, we estimate the plasma specific energy to be[15]

$$\varepsilon = \frac{\gamma(I_0/\rho_0)^{2/3}}{(\gamma^2 - 1)^{1/3}\,(\gamma + 1)} = 2.9 \times 10^{12}\ \text{erg/g}$$

and the plasma temperature to be[17]

$$T = 0.86\left(\frac{\rho}{\rho_0}\right)^{0.08}\left[\frac{\varepsilon(\text{eV/molecules})}{8.3}\right]^{2/3} = 4.2\ \text{eV}$$

The extension of the present laboratory-scale results to long-path transmission in the atmosphere has been numerically studied following standard formulations. An example serves to illustrate the parameter regime where blockage by aerosol-induced plasmas becomes important. Consider a uniform 55-MW/cm^2, 2 μsec (square) pulse propagating through a typical maritime aerosol distribution for which[12]

$$N(>10\ \mu\text{m}) = \int_{10\ \mu\text{m}}^{\infty} r^{-5}\, dr = 2.5 \times 10^{-5}\ \text{cm}^{-3}$$

and assume a 1-km transmission path of unit area (1 cm^2). In this volume there will be two to three particles with radii of 10 μm or larger. A 55-MW/cm^2 beam will produce two to three breakdowns in the subject volume accord-

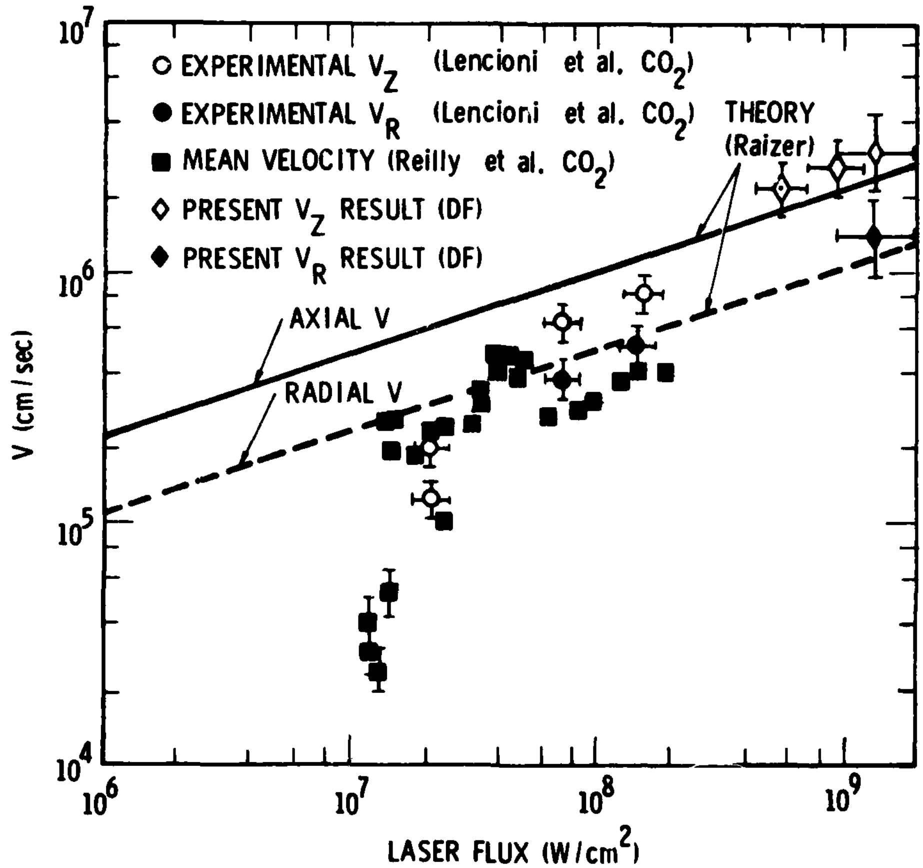

Fig. 9. Plasma Growth Rate for Laser-Irradiated Aerosols

ing to the present breakdown theory (Fig. 6). At this irradiance, the radial expansion velocity is estimated from LSD theory[15] to be

$$v_r = 0.5\left[(\gamma^2 - 1)\,\frac{I_0}{2\rho_0}\right]^{1/3} = 0.5 \text{ cm}/\mu\text{sec} \tag{6}$$

The time for breakdowns to begin is estimated from Fig. 7 to be 0.2 μsec. Since the breakdowns are assumed to originate near the centerline of the spatially uniform beam, the beam becomes fully blocked about 1 μsec after the onset of plasma formation. The fractional energy transmission through the breakdown region can be written as

$$\frac{E_t}{E_i} = \frac{\int_0^{\tau_B} I_0\,dt + \int_{\tau_B}^{\tau_c} I_0\left[1 - (v_r t)^2/r_0^2\right]dt}{\int_0^{\tau_\nu} I_0\,dt}$$

$$= \frac{\tau_B}{\tau_\nu} + \frac{1}{\tau_\nu}\left[(\tau_c - \tau_B) - \frac{v_r^2}{3r_0^2}(\tau_c^3 - \tau_B^3)\right] \tag{7}$$

where τ_B is the onset time for breakdown formation, τ_c is the beam cutoff time, τ_ν is the laser pulse duration, and r_0 is the beam radius. Equation (7) predicts a fractional energy transmission of 31% for the present example. The generalization to nonuniform spatial and temporal beam profiles is easily accommodated. The above calculation relies on a theoretical breakdown threshold estimate for 20-μm-diameter water aerosols. Since the present theory may underestimate breakdown thresholds for water aerosols of large diameter ($\gtrsim$ 20 μm), the fractional energy transmission may exceed the value calculated in the present example. Threshold measurements for intermediate- and large-diameter water aerosols are needed to facilitate reliable predictions of long-path transmission in maritime environments.

IV. CONCLUDING REMARKS

Pulsed DF chain-laser breakdown thresholds have been investigated in water-particle-laden air. Thresholds for fresh- and salt-water aerosols of small (1 to 4 μm) diameter were measured to lie in the range 0.6 to 1.8 GW/cm^2. The apparent large spread in the measured small-particle thresholds was explained on the basis of major differences in laser pulse shapes for two different classes of experiments that were performed. Steeply rising pulses yielded thresholds that were two and one-half to three times greater than the breakdown values observed for flat-topped pulses. Collimated DF beams that encountered large-diameter water particles were incapable of producing breakdowns at irradiance levels of 50 to 59 MW/cm^2 and pulse lengths of 0.5 μsec. Based on threshold scaling as $\tau_\nu^{-1/2}$, we postulate a safe irradiance for a t(μsec)-duration pulse propagating through 100-μm-diameter water particles to be $35[t(\mu sec)]^{-0.5}$ MW/cm^2.

Confidence in the present experimental technique was increased by conducting threshold measurements using 20-μm-diameter alumina particles; the wavelength-scaled HF- and CO_2-laser data of Lencioni et al. have been shown to be in excellent agreement with our alumina threshold measurements. A first attempt was made to construct an empirical correlation of DF breakdown threshold as a function of particle size and time to breakdown. In this correlation, the present data appear to be compatible with our wavelength scaling of the short- and long-pulse data of Lencioni et al. and with clean-air breakdown data of Deka et al.

Plasma growth rate measurements for DF irradiated aerosols have been shown to agree with the theoretical predictions of Razier and are found to be consistent with extrapolations to higher fluences of earlier measurements at CO_2 wavelengths. A plasma temperature of 4.2 eV was inferred from measurements of the axial LSD wave speed at incident irradiances in the neighborhood of 1 GW/cm^2. An approximate theoretical model of the aerosol breakdown process was described that was shown to be in reasonable agreement with the experimental DF data. This model allows scaling of the present laboratory-scale results to long transmission paths in maritime environments. To establish greater confidence in this scaling, we propose that additional measurements, using a larger energy DF laser, are needed to obtain breakdown thresholds for intermediate size (10 to 40 μm diameter) water particles.

REFERENCES

1. D.C. Smith, Appl. Phys. Lett. 19, 405 (1972).

2. G.H. Canavan, W.A. Proctor, P.E. Nielsen, and S.D. Rockwood, IEEE J. Quant. Electron 8, 564 (1972).

3. G.H. Canavan and P.E. Nielsen, Appl. Phys. Lett. 22, 406 (1973).

4. D.E. Lencioni, Appl. Phys. Lett. 23, 12 (1973).

5. D.E. Lencioni, Appl. Phys. Lett. 25, 15 (1974).

6. D.C. Smith and R.T. Brown, J. Appl. Phys. 46, 1146 (1975).

7. D.E. Lencioni, L.C. Pettingill, and D.P. DeGloria, Report No. LTP-35, MIT Lincoln Lab, Oct. 1976.

8. F.V. Bunkin and V.V. Savranskii, Sov. Phys. JETP 38, 1091 (1974).

9. D.B. Nichols and R.B. Hall, J. Appl. Phys. 52, 3851 (1981).

10a. B.K. Deka, P.E. Dyer, D.J. James, and S.A. Ramsden, Opt. Commun. 19, 292 (1975).

10b. M.J. Soileau, Appl. Phys. Lett. 35, 309 (1979).

11. S.T. Amimoto, J.S. Whittier, M.L. Lundquist, F.G. Ronkowski, P.J. Ortwerth, and R. Hofland, "Pulsed Chemical Laser with Variable Pulse-Length E-Beam Initiation and Magnetic Confinement", Appl. Phys. Lett. 40, 20 (1982).

12. G.L. Trusty and T.H. Cosden, "Optical Extinction Predictions from Measurements in the Open Sea," Report No. 8260, NRL, Jan. 1979.

13. R. Hofland, "Pulsed Laser Propagation Through Aerosol Breakdowns: Simple Model," private communication.

14. D. Smith, J. Appl. Phys. 48, 2217 (1977).

15. Y.P. Raizer, Sov. Phys. JETP 21, 1009 (1965).

16. J. Reilly, AIAA Paper 77-697, presented at AIAA 10th Fluid and Plasmadynamics Conf., Albuquerque, N.Mex., 27-29 June 1977.

17. A.I. Larkin, Sov. Phys. JETP 11, 1363 (1960).

☆U.S. Government Printing Office—1982—583-081/2101

LABORATORY OPERATIONS

The Laboratory Operations of The Aerospace Corporation is conducting experimental and theoretical investigations necessary for the evaluation and application of scientific advances to new military space systems. Versatility and flexibility have been developed to a high degree by the laboratory personnel in dealing with the many problems encountered in the nation's rapidly developing space systems. Expertise in the latest scientific developments is vital to the accomplishment of tasks related to these problems. The laboratories that contribute to this research are:

Aerophysics Laboratory: Launch vehicle and reentry aerodynamics and heat transfer, propulsion chemistry and fluid mechanics, structural mechanics, flight dynamics; high-temperature thermomechanics, gas kinetics and radiation; research in environmental chemistry and contamination; cw and pulsed chemical laser development including chemical kinetics, spectroscopy, optical resonators and beam pointing, atmospheric propagation, laser effects and countermeasures.

Chemistry and Physics Laboratory: Atmospheric chemical reactions, atmospheric optics, light scattering, state-specific chemical reactions and radiation transport in rocket plumes, applied laser spectroscopy, laser chemistry, battery electrochemistry, space vacuum and radiation effects on materials, lubrication and surface phenomena, thermionic emission, photosensitive materials and detectors, atomic frequency standards, and bioenvironmental research and monitoring.

Electronics Research Laboratory: Microelectronics, GaAs low-noise and power devices, semiconductor lasers, electromagnetic and optical propagation phenomena, quantum electronics, laser communications, lidar, and electro-optics; communication sciences, applied electronics, semiconductor crystal and device physics, radiometric imaging; millimeter-wave and microwave technology.

Information Sciences Research Office: Program verification, program translation, performance-sensitive system design, distributed architectures for spaceborne computers, fault-tolerant computer systems, artificial intelligence, and microelectronics applications.

Materials Sciences Laboratory: Development of new materials: metal matrix composites, polymers, and new forms of carbon; component failure analysis and reliability; fracture mechanics and stress corrosion; evaluation of materials in space environment; materials performance in space transportation systems; analysis of systems vulnerability and survivability in enemy-induced environments.

Space Sciences Laboratory: Atmospheric and ionospheric physics, radiation from the atmosphere, density and composition of the upper atmosphere, aurorae and airglow; magnetospheric physics, cosmic rays, generation and propagation of plasma waves in the magnetosphere; solar physics, infrared astronomy; the effects of nuclear explosions, magnetic storms, and solar activity on the earth's atmosphere, ionosphere, and magnetosphere; the effects of optical, electromagnetic, and particulate radiations in space on space systems.

LME

8